ELSEVIER

International Journal of Mass Spectrometry 201 (2000) 253–267

International Journal of Mass Spectrometry

Density functional theory predictions for the binding of transition metal cations to pi systems: from acetylene to coronene and tribenzocyclyne

Stephen J. Klippenstein*, Chia-Ning Yang

Chemistry Department, Case Western Reserve University, Cleveland, OH, 44106-7078, USA

Received 26 January 2000; accepted 31 January 2000

Abstract

The Becke-3 Lee-Yang-Parr (B3LYP) density functional is employed in the determination of the structures, binding energies, and vibrational frequencies for the complexes of water, acetylene, ethylene, benzene, $C_{12}H_6$, coronene, and tribenzocyclyne with the first row transition metal cations from Ti through Cu. For the smaller ligands, comparison with the available experimental and theoretical data delineates the accuracy of the B3LYP functional for this type of complex. For acetylene and ethylene, new coupled cluster results provide supplementary comparisons. The B3LYP binding energies are generally within 5 kcal/mol of the corresponding coupled cluster single double (triple) and experimental estimates. The metal coronene binding energies are on average 5 kcal/mol greater than those for the metal benzenes, due simply to the increased polarizability of the ligand. In contrast, the metal ions are much more strongly bound to tribenzocyclyne and $C_{12}H_6$ than to either benzene or coronene (e.g. by 50 kcal/mol). This enhanced binding is related to the large central cavity, which allows for a closer approach of the metal ion to the ligand plane. In fact, the Ni and Cu ions insert directly into the cavity, forming a planar complex, in reasonable agreement with the postulates of an experimental study of Dunbar and co-workers [J. Am. Chem. Soc. 115 (1993) 12477]. (Int J Mass Spectrom 201 (2000) 253–267) © 2000 Elsevier Science B.V.

Keywords: Metal Pi bonding; density functional theory; quantum chemistry M^+(TBC); 7^+(Poronene); B3LYP

1. Introduction

The relatively modest computational requirements of density functional theory (DFT) make it an attractive method for obtaining molecular properties of metal–ligand complexes, particularly for larger species and multiply ligated complexes. Quantitatively accurate estimates for properties such as the vibrational frequencies, infrared absorption intensities, and rotational constants are often of value in the extraction of thermodynamic data such as the binding energies from kinetic modeling of experimental data. The Becke-3 Lee-Yang-Parr (B3LYP) [1] density functional (among others) generally provides estimates for these properties which are more accurate than the values obtained with the much more computationally demanding second order Møller-Plesset (MP2) perturbation theory.

Various recent studies suggest that the B3LYP estimated cationic metal–ligand binding energies are also at least qualitatively correct, with a maximum

* Corresponding author.

PII S1387-3806(00)00221-9

discrepancy of about 6 kcal/mol (see, e.g. [2–8]). Furthermore, B3LYP calculations have been found to provide a useful indication of trends among different ligands and between different transition metals. For $M(CO_2)^+$ the B3LYP binding energies were consistently about 3–4 kcal/mol greater than the coupled cluster single double (triple) [CCSD(T)] ones [3]. For cationic transition metal–benzene complexes, the B3LYP estimates [6] for the binding energies were generally within 2 kcal/mol (for all but Ti and V, where the discrepancy is about 6 kcal/mol) of those extracted from the kinetic modeling of collision-induced dissociation experiments [9], while the agreement with MCPF quantum chemical calculations [10] was even better. The B3LYP predictions for the trends in the binding of Cr cation to a complete set of fluoro-benzenes ($C_6F_xH_{6-x}$, x = 1–6) were in similarly good agreement with radiative association kinetic modeling results, with a maximum discrepancy of about 5 kcal/mol [7]. For pyrrole similar discrepancies exist for the transition metals, but for Mg^+ and Al^+ the discrepancy is as large as 8 kcal/mol [8]. A valuable study of the discrepancies between DFT and more traditional quantum chemical estimates {e.g. MP2 and quadratic configuration interaction with perturbative inclusion of triple excitations [QCISD(T)]} was provided by Schwarz and co-workers for cationic Al complexes [11].

In this work, we explore the accuracy of B3LYP estimated cationic transition metal–ligand binding energies for a variety of π containing ligands, and also make predictions for a few larger ligands. The specific ligands considered are H_2O, C_2H_2, C_2H_4, C_6H_6, $C_{12}H_6$, and two forms of $C_{24}H_{12}$; coronene and tribenzocyclyne. For each ligand, B3LYP estimates for the binding properties (energies, structures, and vibrational frequencies) are obtained for each of the first row transition metal cations from Ti through Cu. The nonelectrostatic component of the bonding in these complexes primarily involves the interaction of the metal *d* orbitals with the π and π^* orbitals of the ligands (or more precisely the lone pair orbitals for the water ligand). The variation of the π-orbital environment throughout the series should provide a fairly robust test of the density functional methodology for this type of complex.

In a seminal series of studies Bauschlicher and co-workers examined the binding of the transition metal cations to H_2O, C_2H_2, C_2H_4, and C_6H_6 via the modified coupled pair functional (MCPF) methodology [10,12–16]. Here, we supplement their results for the C_2H_2, and C_2H_4 ligands with additional couple cluster calculations, partly because the present B3LYP results suggest significant deviations from the self-consistent field (SCF) geometries employed in these earlier MCPF studies. For the H_2O ligand QCISD(T) and CCSD(T) calculations were reported in [17] and [18], respectively. The binding energies for these same metal–ligand complexes have been examined in a series of collision-induced dissociation experiments by Armentrout and co-workers [9,19–21]. Two other experimental studies have also estimated the binding energies for the $M(H_2O)^+$ complexes [22,23]. Comparison of the present density functional estimates with these experimental and theoretical results serves to further delineate the expected level of accuracy for the application of the B3LYP functional to the binding of related ligands, such as the $C_{12}H_6$ and $C_{24}H_{12}$ ligands studied here.

The coronene and tribenzocyclyne (TBC) ligands have been the subject of radiative association kinetics studies in the Dunbar group [24–26]. The coronene ligand consists of six benzene rings surrounding a central benzene ring (cf. Fig. 1). Its binding might be expected to be similar to that of benzene, with only a modest increase in the strength of the binding due to an increased molecular polarizability. In contrast, the TBC ligand (cf. Fig. 1) consists of three benzene ligands joined by three acetylene groups to form a planar moiety with a moderately large central cavity. For this ligand it may be possible for the metal cation to insert into the central cavity. In fact, the variation in the efficiency of forming dimers led Dunbar and co-workers to suggest that the Co, Ni, and Cu cations insert into the cavity, while the remaining first row transition metal cations do not [25]. Density functional theory, with its generally accurate geometries and semiquantitatively correct binding energies, pro-

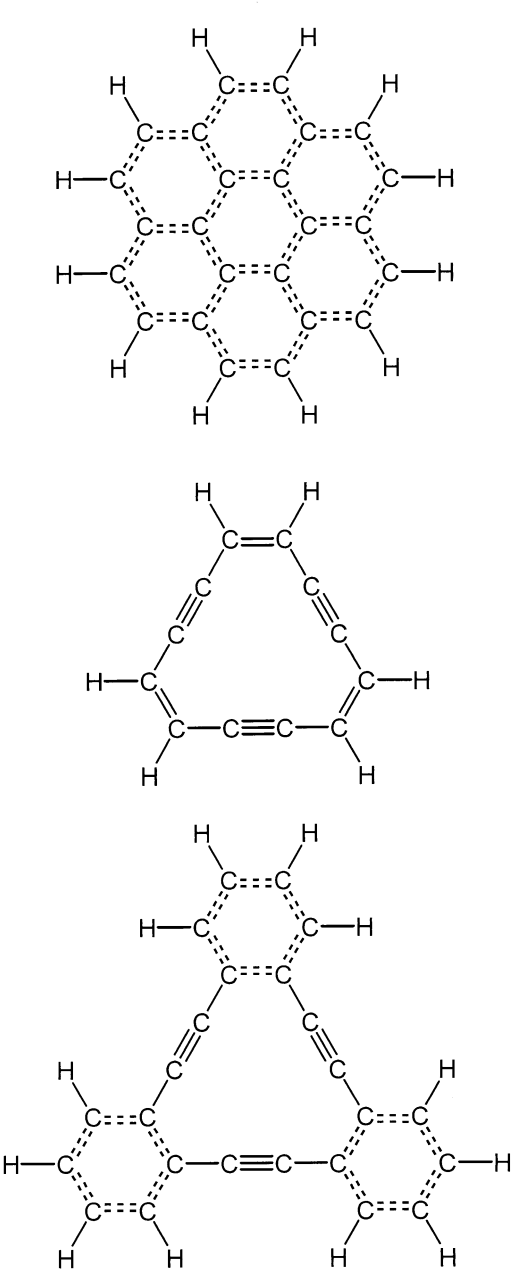

Fig. 1. Structures of coronene, $C_{12}H_6$, and tribenzocyclyne, from top to bottom, respectively.

vides an ideal means for examining the feasibility of such a cavity insertion process.

The $C_{12}H_6$ ligand studied here (cf. Fig. 1), corresponds to replacing the three benzene moieties of TBC with ethylene groups, and appears to be a purely theoretical construct. The resulting ligand is similar in nature to the TBC ligand, but is considerably smaller, making it useful as an intermediate stage to the examination of the binding for the full TBC ligand. Furthermore, it is interesting to consider whether the minor variation in cavity structure from tribenzocyclyne to $C_{12}H_6$ affects the cavity formation process.

2. Quantum chemical methodology

The B3LYP hybrid density functional [1] is employed in the determination of optimized structures and vibrational frequencies for each of the complexes and free ligands. For acetylene and ethylene, coupled cluster calculations were also performed including single and double excitations and perturbative estimates of the triplet contributions [CCSD(T)]. These single point CCSD(T) calculations were performed at the B3LYP optimized geometries. The GAUSSIAN94 and GAUSSIAN98 quantum chemical packages [27] were employed in these evaluations.

Four separate basis sets were employed in various aspects of this work. The smallest basis set (B1) consists of the 6-311G basis for the metal cations, and the 3-21G basis for the C and H atoms. This basis set was employed in the geometrical optimizations and frequency analyses for the larger ligands ($C_{12}H_6$ and $C_{24}H_{12}$). The next larger basis set (B2), consisting of the 6-311+G* basis set for the metals and the 6-31G* basis for the C, O, and H atoms, was employed in the optimizations and frequency analyses for the remaining ligands, as well as in the CCSD(T) evaluations. This 6-311+G* metal basis includes a single set of *f* polarization and *s*-, *p*-, *d*-diffuse functions in addition to the standard 6-311G basis set [27]. For the benzene and smaller ligands, final B3LYP energetic estimates were obtained at the optimized geometries employing basis set (B3), which differs from basis set B2 only in the addition of diffuse *s* and *p* functions to the C and O atoms. Sample evaluations suggest that, with the B3LYP functional, any basis set superposition errors are less than 1 kcal/mol for this basis set.

Such a correction was considered to be of negligible importance for the present analyses. Basis set B3′, in which the diffuse functions were added to only the six C atoms nearest to the metal, was instead employed in the final B3LYP estimates for the $C_{12}H_6$ and $C_{24}H_{12}$ ligands.

In the B3LYP calculations, there is essentially no spin contamination when considering states that correlate with the ground state of the ion. For states of a different spin or different configuration, the contamination is still small but not necessarily insignificant. In particular, for the ^{3}V, ^{4}Cr, ^{5}Mn, and ^{4}Fe states of the complexes the spins are as high as 2.05, 3.87, 6.15, and 3.80, respectively.

The optimizations for the $M(C_6H_6)^+$, $M(C_{12}H_6)^+$, and $M(C_{24}H_{12})^+$ complexes considered only T-shaped geometries, with the metal approaching perpendicularly to the plane of the ligand. For the metal–benzene and metal–coronene complexes the optimized geometries were generally of C_{6v} symmetry. However, orbital degeneracies would sometimes result in a Jahn-Teller induced reduction to C_{2v} symmetry. Similarly, for the $M(C_{12}H_6)^+$ and $M(TBC)^+$ complexes Jahn-Teller distortions occasionally result in a reduction from C_{3v} to C_s symmetry.

The B3LYP/B2 estimated zero-point corrections (with no scale factors) are employed for both the B3LYP/B3 and CCSD(T)/B2 binding energy evaluations. The B3LYP/B3′ binding energies employ the B3LYP/B1 estimated zero-point corrections. When imaginary frequencies were encountered, those frequencies were set to zero in estimating the zero-point energy.

Estimates of the effect of core correlation and basis set limitations were performed at the MP2 level treating all electrons as active and employing the 6-311++G(2df,2pd) basis set. For the most part such calculations suggested only minor corrections (i.e. 1–2 kcal/mol) to the CCSD(T)/B2 results. Furthermore, incorporating such corrections actually worsens the agreement between the calculated and experimental free ion excitation energies. Thus, such corrections are not reported here.

3. Results and discussion

3.1. Free metal ion energies

For a number of the complexes the metal ion configuration in the ground electronic state differs from that of the ground state of the free metal ion. In these cases, the overall binding energy depends to some extent on the electronic excitation energy of the free metal ion. Unfortunately, obtaining an adequate description of such excitation energies is a difficult quantum chemical problem and the B3LYP density functional is not especially well suited for this. The present B3LYP/B3 and CCSD(T)/B2 calculated electronic excitation energies for the first row transition metal cations are reported in Table 1 together with the corresponding experimental [28] and MCPF [29] excitation energies. Related QCISD(T) [30] results are closely analogous to these CCSD(T) results, while the present B3LYP results mimic earlier density functional values [31–34].

The relatively large errors for the B3LYP/B3 results are simply the result of overestimating the stability of the d^n configuration relative to the $d^{n-1}s$ configuration. For the Ti and Fe cations, this overestimate, which is 7 kcal/mol on average, even results in an incorrect prediction of the ground state for the free ion. In contrast, the CCSD(T)/B2 method tends to underestimate the d^n stability, but to a much lesser extent.

Inaccurate estimates for the free ion state splittings are parlayed into errors for the corresponding states of the complex. One approximate remedy for this situation is to evaluate the binding energy for the diabatic dissociation process and to adjust this back to the ground state to ground state dissociation energy via the experimental [28] free ion splitting. This remedy was employed for all the B3LYP/B3 and CCSD(T)/B2 results, presented here.

In some cases, e.g. the $^4Ti(L)^+$ states, the ground state of the complex is a roughly equal admixture of d^n states and $d^{n-1}s$ states. In these cases, we have examined the Mulliken populations to determine which state makes the greater contribution and considered the diabatic dissociation for that state. Alter-

Table 1
Electronic excitation energies for transition metal cations

			Expt.[b]	B3LYP[c]		CCSD(T)[d]		MCPF[e]	
M^+	State	Config.[a]	E	E	ΔE	E	ΔE	E	ΔE
Ti	^4F	$3d^2(^3F)4s$	0	0		0			0
	^4F	$3d^3$	2.5	−5.1	**−7.6**	4.1	**1.6**	4.6	**2.1**
	^2F	$3d^2(^3F)4s$	13.0						
	^2D	$3d^2(^1D)4s$	24.3	49.2	**24.9**	33.7	**9.4**		
	^2F	$3d^3$	25.3	26.7	**1.4**	36.4	**11.1**		
V	^5D	$3d^4$	0	0		0			
	^5F	$3d^3(^4F)4s$	7.8	12.8	**5.1**	6.4	**−1.4**	7.1	**−0.7**
	^3F	$3d^3(^4F)4s$	24.9						
	^3P	$3d^4$	32.9	37.4	**4.5**	40.9	**8.0**		
	^3H	$3d^4$	35.5						
	^3F	$3d^4$	38.2						
	^5P	$3d^3(^4P)4s$	38.4						
	^3G	$3d^4$	41.1						
	^3G	$3d^3(^2G)4s$	46.4	60.6	**14.2**	56.0	**9.5**		
Cr	^6S	$3d^5$	0	0		0			
	^6D	$3d^4(^5D)4s$	35.1	39.0	**3.9**	37.2	**2.0**	39.2	**4.1**
	^4S	$3d^4(^5D)4s$	56.7						
	^4G	$3d^5$	58.7	56.3	**−2.4**	68.9	**10.2**		
Mn	^7S	$3d^5(^6S)4s$	0	0		0			
	^5S	$3d^5(^6S)4s$	27.1						
	^5D	$3d^6$	41.7	27.9	**−13.8**	47.6	**5.9**	49.1	**7.4**
Fe	^6D	$3d^6(^5D)4s$	0	0		0			
	^4F	$3d^7$	5.7	−5.0	**−10.8**	7.8	**2.0**	9.2	**3.5**
Co	^3F	$3d^8$	0	0		0			
	^5F	$3d^7(^4F)4s$	9.9	17.3	**7.4**	8.6	**−1.3**	6.9	**−3.0**
Ni	^2D	$3d^9$	0	0		0			
	^4F	$3d^8(^3F)4s$	25.0	28.5	**3.5**	24.5	**−0.5**	22.6	**−2.4**
Cu	^1S	$3d^{10}$	0	0		0			
	^3D	$3d^9(^2D)4s$	64.8	68.7	**4.0**	71.3	**6.6**	69.6	**4.8**

[a] Electronic configuration.
[b] Experimental *j*-averaged excitation energy from [28].
[c] Present B3LYP/B3 excitation energies and errors relative to experiment (bold) in kcal/mol.
[d] Present CCSD(T)/B2 excitation energies and errors relative to experiment (bold) in kcal/mol.
[e] MCPF results from [29].

natively, one might employ an average of the results for the two different diabatic processes. However, doing so leads to B3LYP and CCSD(T) results which are generally less consistent with each other and with experiment and so this alternative was not employed here. A meaningful averaged correction may require a better estimate of the *s* and *d* populations than provided by the Mulliken populations.

3.2. H_2O, C_2H_2, and C_2H_4

The present B3LYP estimated metal–ligand binding energies and separations are provided in Tables 2–4 for the H_2O, C_2H_2, and C_2H_4 ligands, respectively. The results of various related theoretical and experimental studies are also summarized therein. The qualitative description of the bonding provided

Table 2
Metal ligand binding energies and separation for $M(H_2O)^+$

		Binding energy (kcal/mol)[a]					R_{MO} (Å)[b]				
M^+	State	MCPF[c]	CC[d]	QC[e]	B3LYP[f]	Expt.[g]	UHF[h]	MCPF[c]	MP2[i]	QC[e]	B3LYP[f]
Ti	$^4B_1$	37.5	36.4	39.4	44.0	**36.8** (38.0)	2.165	2.135	2.114	2.131	2.088
	$^4B_2$	37.3	35.6		44.3			2.137			2.099
	$^4A_2$		28.1		28.6						
V	$^5A_1$	34.7	41.8	32.2	38.7	**35.1** (36.2) 28.1	2.192	2.091	2.069	2.103	2.086
	$^5A_2$	34.6	41.6		38.2			2.092			2.084
	$^5B_2$	33.2			38.5			2.051			2.056
	$^5B_1$	28.7			34.0			2.1			2.124
Cr	$^6A_1$	30.1	30.7	32.1	34.9	**30.8** (29.0) 21.9	2.232	2.146	2.115	2.146	2.072
Mn	$^7A_1$	28.5	27.7	32.9	30.0	**28.4** (32.5) 27.0	2.224	2.200	2.206	2.207	2.159
	$^5A_1$	<-14	12.0		-5.6						
Fe	$^6A_1$	33.7	32.1	32.1	35.0	**30.6** (28.8) 32.7	2.176	2.115	2.117	2.126	2.079
	$^6A_2$	33.7			35.2						2.081
	$^6B_2$				32.8						2.090
	$^4A_1$	29.3	33.5		33.4			2.002			1.991
	$^4B_1$		30.0		33.6				2.019		1.992
	$^4B_2$		27.7		31.9						2.034
Co	$^3B_2$	38.2	37.1	36.3	40.7	**38.5** (37.1) 29.1	2.106	1.992	1.973	2.036	1.960
	$^3A_2$	37.5	37.5		40.2			2.026	2.003		1.985
	$^3A_1$	37.5	37.4		40.2						1.988
	$^3B_1$	36.4			38.0						1.992
Ni	$^2A_1$	41.1	36.3	38.6	45.0	**43.0** (36.5) 37.1	2.094	1.975	1.952	1.972	1.943
	$^2B_2$	39.3	34.9		42.4			1.971			1.932
	$^2A_2$	37.2			40.4			1.958			1.945
	$^2B_1$				38.8						1.988
Cu	$^1A_1$	37.3	36.2	36.0	41.3	**37.5** (35.0)	2.060	1.973	1.945	1.975	1.938

[a] Zero-point corrected metal ligand binding energies.
[b] Equilibrium metal oxygen separation in the $M(H_2O)^+$ complex.
[c] MCPF results from [12].
[d] CCSD(T)(full)/6-311++G**//MP2(full)/6-311++G** results from [18].
[e] QCISD(T)/Bausch results from [17], where Bausch denotes a $(14s11p6d1f/8s6p4d1f)$ contraction.
[f] Present B3LYP/B3//B3LYP/B2 results including B3LYP/B2 zero-point correction.
[g] Experimental results from [19] (bold), [22] (in parentheses) and [23].
[h] UHF/Bausch results from [17].
[i] MP2(full)/6-311++G** results from [18].

by Bauschlicher and co-workers in [12–16] provides an important framework for understanding these binding energies. For brevity we refrain from repeating this description and instead refer the interested reader to those references. For ease of comparison we utilize their symmetry notation even though, for the H_2O ligand, this corresponds to a reversal of the B_1 and B_2 symmetry labels from that output by GAUSSIAN.

For the $M(H_2O)^+$ complexes the agreement between the experimental results of Armentrout and co-workers [19] and the MCPF results of Bauschlicher and co-workers [12] is remarkable; only for Fe and Ni is the discrepancy greater than 0.7 kcal/mol and even for those two it is only 3.1 and 1.9 kcal/mol, respectively. The B3LYP predicted binding energies are consistently a few kcal/mol greater than these, ranging from 1.6 to 7.2 kcal/mol greater than the experimental results, and being 3.6 kcal/mol greater

Table 3
Metal ligand binding energies and separation for $M(C_2H_2)^+$

		Binding energy (kcal/mol)[a]				R_{MX} (Å)[b]	
Metal	State	MCPF[c]	CC/B2[d]	B3LYP[e]	Expt.[f]	SCF[g]	B3LYP[e]
Ti	$^2A_2$	39.1	52.9	56.0	60.5	1.86	1.818
	$^2A_1$	38.0	51.1	53.8		1.89	1.853
	$^4B_1$	21.1	29.6	34.1		2.60	2.124
	$^4B_2$	19.1	27.1	33.8		2.72	2.136
V	$^3A_2$	27.3	39.1	44.4	49.0	1.89	1.802
	$^5A_1$	24.1	29.6	33.8		2.56	2.186
	$^5B_1$		29.9	34.9			2.113
Cr	$^6A_1$	19.8	25.7	29.5	44.0	2.59	2.231
	$^4B_2$	−27.5	1.1	2.5		2.20	1.882
	$^4A_2$		9.1	9.4			1.781
Mn	$^7A_1$	14.4	19.6	18.1		2.78	2.592
	$^5B_2$	−7.2	19.2	16.5		2.21	1.880
Fe	$^4B_2$	23.1	39.3	42.6		2.32	1.912
	$^6B_2$		23.7	23.0			2.369
	$^6A_2$			22.7			2.495
	$^6A_1$	18.7	22.7	21.7		2.66	2.497
Co	$^3B_1$	32.3	44.4	47.4	>6.5	2.31	1.895
	$^3A_1$	32.1	41.6	45.8		2.32	1.960
Ni	$^2A_1$	34.3	44.6	48.0	>1.7	2.28	1.937
	$^2B_1$		44.6	48.6			1.883
Cu	$^1A_1$	32.0	40.3	43.9	>2.4	2.25	1.991

[a] Zero-point corrected metal ligand binding energies.
[b] Equilibrium distance from the metal to the CC bond midpoint in the $M(C_2H_2)^+$ complex.
[c] MCPF results from [14] including constant zero-point correction of −0.8 kcal/mol.
[d] Present CCSD(T)/B2//B3LYP/B2 results including B3LYP/B2 zero-point correction.
[e] Present B3LYP/B3//B3LYP/B2 results including B3LYP/B2 zero-point correction.
[f] Experimental results from [20].
[g] SCF results from [14].

on average. The underprediction of the equilibrium metal–ligand separation in the B3LYP calculations relative to the MCPF ones is likely correlated with its overprediction of the binding energies. For Co and Ni, the B3LYP predicted splitting between the different states of the same spin is in reasonable agreement with the available MCPF results. For Ti, V, and Fe, the increased discrepancies in the calculated state splittings are likely related to differences in the calculated $d^{n-1}s$ to d^n excitation energies, since the various states have varying degrees of s–d mixing.

As might be expected both the QCISD(T)/Bausch results from [17] and the CCSD(T)(full)/6-311++G** binding energies of [18] are closely analogous to the MCPF results; generally differing by 2 kcal/mol or less. However, for V and Ni the CCSD(T) values differ from the MCPF values by inordinately large amounts of 7.1 and 4.8 kcal/mol, respectively. Sample calculations suggest that the V^+ energy used in the CCSD(T) study was erroneously low, with a corrected binding energy of 35.6 kcal/mol for the $^5A_1$ state once again being within 1 kcal/mol of the MCPF results. We have no explanation for the deviations in the Ni case.

For the acetylene ligand there is a close correspondence between the present B3LYP and CCSD(T)

Table 4
Metal ligand binding energies and separation for $M(C_2H_4)^+$

		Binding Energy (kcal/mol)[a]				R_{MX} (Å)[b]	
Metal	State	MCPF[c]	CCSD(T)[d]	B3LYP[e]	Expt.[f]	SCF[g]	B3LYP[e]
Ti	$^2A_1$	24.2	34.4	37.8	34.8	2.03	1.926
	$^4B_1$		26.7	30.2			2.281
	$^4B_2$	19.0		27.4		2.82	2.267
V	$^5A_1$	24.2	28.2	32.3	29.8	2.69	2.267
	$^3A_2$	9.5	19.2	23.5		2.07	1.951
Cr	$^6A_1$	20.9	26.1	30.1	22.8	2.60	2.279
	$^4B_2$	−28.1	−4.4	−2.9		2.26	1.930
	$^4A_2$			−15.3			1.949
Mn	$^7A_1$	15.5	19.9	18.8	21.7	2.82	2.663
	$^5B_2$	−7.5	13.4	12.6		2.26	1.949
	$^5A_1$	*−13.8*		−2.5[h]			2.322
	$^5A_2$	*−14.3*		−10.2			2.289
	$^5B_1$	*−14.3*		−9.7			2.267
	$^5A_1$	*−15.0*					
Fe	$^4B_2$	24.6	38.7	41.8	34.6	2.34	1.980
	$^6A_1$	19.9	24.1	23.6		2.70	2.577
Co	$^3A_2$	35.1	43.9	47.6	44.5	2.31	1.974
	$^3A_1$			46.8			1.988
	$^3B_1$	33.8		44.8			2.012
Ni	$^2A_1$	36.2	45.0	49.1	43.6	2.29	1.991
	$^2B_1$	*34.1*		45.5			2.012
	$^2A_2$	*33.9*		47.5			1.986
	$^2A_1$	*33.7*					
	$^2B_2$	*32.1*		38.3			2.183
Cu	$^1A_1$	34.6	42.2	46.5	42.0	2.25	2.012

[a] Zero-point corrected metal–ligand binding energies.
[b] Equilibrium distance from the metal to the CC bond midpoint in the $M(C_2H_4)^+$ complex.
[c] MCPF results from [15] including the present B3LYP/B2 zero-point correction. The numbers in italics for Mn and Ni correspond to the Complete Active Space SCF (CASSCF) energy splittings added on to the MCPF energy for the $^5B_2$ state.
[d] Present CCSD(T)/B2//B3LYP/B2 results including B3LYP/B2 zero-point correction.
[e] Present B3LYP/B3//B3LYP/B2 results including B3LYP/B2 zero-point correction.
[f] Experimental results from [21].
[g] SCF results from [15].
[h] The average spin squared for this state is 6.41, indicating a considerable spin contamination.

calculations, with average and maximum discrepancies of 3.2 and 6.7 kcal/mol, respectively. In each case, the B3LYP predicted binding energy exceeds the CCSD(T) one, and yet the B3LYP values underestimate the experimental binding energies [20] for Ti, V, and Cr, by 4.5, 4.4, and 14.5 kcal/mol, respectively. It is unclear why there is such a large discrepancy between theory and experiment for these cases.

There is an even greater discrepancy between the present calculations and the MCPF results from [14], with the present CCSD(T) predicted binding energies for the ground state of the complex exceeding the corresponding MCPF values by 10.5 kcal/mol on average. Much of this discrepancy can be explained by the much shorter (typically by about ∼0.3–0.4 Å) equilibrium metal-ligand separation for the present B3LYP results as opposed to the SCF geometries employed in the MCPF calculations of [14]. The much larger binding energies for the present

CCSD(T) results, which employ the B3LYP geometries, suggests that the B3LYP geometries are closer to the true equilibrium values.

For $Ti(C_2H_2)^+$ and $V(C_2H_2)^+$ the B3LYP and CCSD(T) geometries are reasonably similar and yet the CCSD(T) and MCPF binding energies are still very different. For these cases, the explanation lies in the present calculation of the dissociation energy via the diabatic dissociation process coupled with a correction by the experimental promotion energy for the free ion. This procedure results in corrections of 11.1 and 8.0 kcal/mol for the Ti and V binding energies, respectively. For Fe, and for the excited states of Cr and Mn, both the geometrical and diabatic dissociation effects are an important component of the differences.

The results for the metal–ethylene complexes are qualitatively very similar to those for the metal–acetylene complexes. In particular, there is again reasonable agreement between the B3LYP and CCSD(T) binding energies, with a nearly constant difference of 4 kcal/mol between them (for the ground state of the complexes). Furthermore, the MCPF predicted binding energies [15] are once again much lower than the CCSD(T) predictions, due to major differences in the B3LYP and SCF predicted metal–ligand separation, and due to the present diabatic based treatment of the dissociation process.

However, there is a significant difference, in that the experimental results [21] for the $M(C_2H_4)^+$ binding energies are more complete, and the CCSD(T) results are in good agreement with them, differing by only 1.7 kcal/mol on average. This good agreement suggests that the present use of a somewhat limited basis set (i.e. basis set B2) has only a minor effect on the CCSD(T) prediction of the binding energies. Furthermore, it indicates that the differences between the CCSD(T) and MCPF results are truly indicative of failures in the MCPF estimates, i.e. in the use of the SCF geometries.

The B3LYP/B2 estimated vibrational frequencies for each of the ground states of the $M(H_2O)^+$, $M(C_2H_2)^+$, and $M(C_2H_4)^+$ species are reported in Table 5. In each case, the lowest three frequencies correspond to those for the metal–ligand motions. For most cases, the remaining modes vary only slightly from those for the free ligand. However, for the $Ti(C_2H_2)^+$, $Ti(C_2H_4)^+$, and $V(C_2H_2)^+$) species, a number of other frequencies are quite different. These variations also correlate with variations in the CC bond lengths and are indicative of stronger covalent interactions for these species, as indicated in [14] and [15].

3.3. C_6H_6 and coronene

The present B3LYP results for the metal–benzene and metal–coronene [$M(Cor)^+$] binding energies are reported in Table 6. The MCPF [10] and experimental collision-induced dissociation modeling [6,9] results for the metal-benzene binding energies are also provided therein. Once again, within their MCPF study, Bauschlicher and co-workers have provided a valuable qualitative description of the bonding in metal benzene cations [10]. Here, we assumed that the orbital orderings were the same in the metal–coronenes as in the metal–benzenes.

As noted in [6], there is a good correspondence between B3LYP and MCPF predictions for the metal benzene binding energies, with the two predictions differing by more than 2 kcal/mol for only Ti and Fe. For the metal–ligand separations, the variations are more significant, with the greatest discrepancies for Ti, Fe, and Co. The latter three ions correspond to cases where a mixing of the F and P free ion states is required to form the ground states of the complex. Apparently, there is some difference in the B3LYP and MCPF treatments of this mixing.

The B3LYP and MCPF estimates are also in reasonable agreement with the experimental data, with only the Ti and V predictions differing by more than 4 kcal/mol. For Ti, some of the underestimate in the theoretical predictions may be an indication that the experiments are actually observing the diabatic dissociation process. If so, the experimental value would be lowered by 2.5 kcal/mol.

On average, the metal coronene binding energies are 5 kcal/mol greater than the metal–benzene binding energies. However, there is considerable variation in the difference between the two. Interestingly, a correlation between this difference and the metal–ligand separation exists, as illustrated in Fig. 2. At

Table 5
Vibrational frequencies for the ground electronic states of $M(H_2O)^+$, $M(C_2H_2)^+$, and $M(C_2H_4)^+$[a]

Metal	$M(H_2O)^+$	$M(C_2H_2)^+$	$M(C_2H_4)^+$
Ti	363,402,565,1703,3675,3756	589,619,701,797,848,1042, 1490,3202,3229	431,444,497,664,796,902,965,1131, 1200,1429,1473,3086,3092,3157,3176
V	187,391,553,1693,3687,3772[b]	563,584,706,773,829,975, 1562,3222,3257	262,273,421,833,976,992,1028,1263, 1325,1488,1614,3137,3143,3231,3235
Cr	211,390,559,1698,3704,3787	256,284,591,654,760,787, 1976,3349,3443	226,263,386,839,1002,1037,1053,1243, 1350,1488,1631,3139,3145,3221,3241
Mn	305,334,514,1690,3644,3737	73,185,588,660,779,851, 2035,3370,3473	97,181,312,841,994,1058,1060,1247,1364, 1487,1648,3121,3166,3205,3259[c]
Fe	260,368,533,1678,3635,3729	411,425,691,737,756,781, 1841,3295,3368	327,357,521,824,974,1000,1008,1228,1277, 1470,1566,3128,3132,3210
Co	−78,427,611,1696,3691,3774[d]	379,413,628,742,745,785, 1867,3306,3387	312,339,515,835,1015,1020,1038,1230, 1301,1482,1588,3129,3134,3212,3231
Ni	25,433,625,1695,3693,3781[b]	351,372,616,727,764,806, 1911,3325,3410	310,339,522,833,1012,1029,1048,1226, 1305,1484,1596,3139,3143,3217,3240
Cu	106,413,611,1686,3692,3782[b]	291,340,592,709,784,828, 1958,3338,3431	262,314,472,839,1034,1055,1066,1241, 1333,1488,1611,3142,3146,3228,3247

[a] The frequencies are in cm^{-1}, and, unless specified otherwise, are for B3LYP/B2 calculations in C_{2v} symmetry.
[b] The reported frequencies are for basis set B3 since those for basis set B2 contained an imaginary frequency.
[c] These frequencies are for C_s symmetry.
[d] Attempts to locate a lower energy stationary point in C_s symmetry failed and calculations with the B3 basis set also produced one imaginary frequency.

large separation the increased polarizability of the coronene ligand yields somewhat greater binding energies for the metal–coronenes. However, as the separation decreases, covalent interactions become more important. These covalent interactions are similar in the two ligands (or, perhaps, more attractive in the metal benzene species) and so the binding energies become more similar.

The metal–ligand separations are also somewhat greater (on average) in the metal–coronene complexes. However, much of this difference is simply the result of the difference between optimizations with the B1 and B2 bases. For example, optimizing $Cu(C_6H_6)^+$ with the B1 basis yields an R_{MX} separation of 1.883 Å, which is now greater than that in $Cu(coronene)^+$. The complexation process produces only modest changes in the internal structure of the coronene ligand. For example, the out-of-plane displacements, which appear to correspond to the greatest structural change, are generally restricted to a few hundredths of an angstrom [35].

Harmonic vibrational analyses have been performed for each of the ground state complexes [35]. For the metal–coronene species, in many instances (i.e. V, Cr, ^{4}Fe, Ni, and Cu) one or more of the frequencies was imaginary, suggesting some deviation from the symmetry considered in the optimization. However, in each instance, related vibrational analyses for the metal–benzene species indicated that the imaginary frequencies are simply the result of limitations in the B1 basis set. Thus, no further optimizations in a lower symmetry group were performed.

The present B3LYP predictions for the cationic metal–coronene binding energies are in agreement with the qualitative observations made in the radiative association kinetics study of Pozniak and Dunbar [24]. In particular, for each metal species the binding energy exceeds the 35 kcal/mol necessary to produce the observed efficient radiative stabilization. Furthermore, additional calculations for the $Na(coronene)^+$ species, suggest that its binding energy is only 32.0 kcal/mol, which is reasonably close to the suggested

Table 6
Metal ligand binding energies and separation for $M(C_6H_6)^+$ and M(coronene)$^+$

			Binding energy (kcal/mol)[a]				R_{MX} (Å)[b]		
Metal	State	Sym.	$M(C_6H_6)^+$ MCPF[c]	B3LYP[d]	Expt.[e]	$M(Cor)^+$ B3LYP[f]	$M(C_6H_6)^+$ MCPF[c]	B3LYP[d]	$M(Cor)^+$ B3LYP[f]
Ti	$^4A_1$	C_{6v}	59.8	55.8	65.1	52.1	2.059	1.883	1.935
	$^2A_2$	C_{2v}		45.1				1.747,1.610	
V	$^5B_2$	C_{2v}	50.7	48.8	56.4	53.5	1.964	1.961,1.929	2.044,2.002
	$^3A_2$	C_{2v}		48.3				1.727,1.588	
Cr	$^6A_1$	C_{6v}	36.7	37.4	40.5	46.2	2.110	2.104	2.125
	$^4B_2$	C_{2v}		9.4				1.781,1.590	
Mn	$^7A_1$	C_{6v}	34.3	32.4	32.1	42.6	2.300	2.360	2.303
	$^5A_1$	C_{2v}		14.1				1.837,1.741	
Fe	$^4A_1$	C_{2v}		49.2	49.9	56.0		1.826,1.767	1.920,1.881
	$^4A_1$	C_{6v}	46.4	39.6		33.2	1.830	1.665	1.722
	$^6A_1$	C_{2v}	40.5	39.6		49.9	2.153	2.207,2.196	2.208,2.205
Co	$^3A_1$	C_{6v}	61.6	60.0	64.0	59.3	1.854	1.663	1.712
Ni	$^2B_2$	C_{2v}	58.8	58.7	58.0	64.4	1.750	1.715	1.796,1.746
Cu	$^1A_1$	C_{6v}	50.4	50.3	50.6	59.7	1.852	1.848	1.874

[a] Zero-point corrected metal ligand binding energies.
[b] Equilibrium distance from the metal to the plane containing the first ring of carbon atoms. For C_{2v} symmetry, two numbers are provided, with the first corresponding to the distance to the fourfold degenerate carbons and the second to the twofold degenerate carbons.
[c] MCPF/DZ2P results from [10], including the present B3LYP/B2 estimate for the zero-point correction.
[d] Present B3LYP/B3//B3LYP/B2 results which are essentially identical to the B3LYP results from [6]. The zero-point corrections are evaluated with the B2 and B1 basis sets for benzene and coronene, respectively.
[e] Experimental collision-induced dissociation modeling results [6,9].
[f] Present B3LYP/B3′//B3LYP/B1 results.

maximum of about 25 kcal/mol required to explain its slow production. In contrast, the radiative association of Na^+ with TBC is readily observed [25], and we calculate its binding energy to be significantly greater, i.e. 46.3 kcal/mol (see Fig. 2).

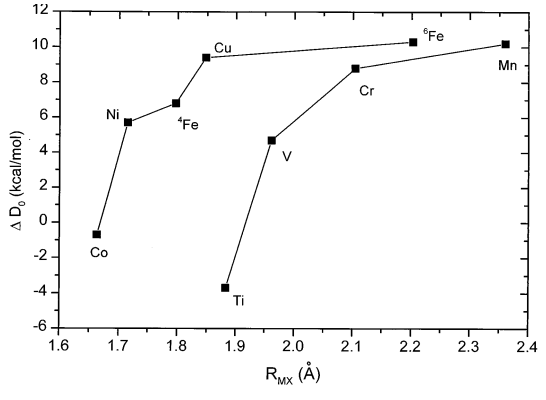

Fig. 2. Difference between the cationic metal–coronene and metal–benzene binding energies vs. metal–ligand separation distance.

3.4. $C_{12}H_6$ and tribenzocyclyne

The TBC ligand is a relatively novel ligand with a cavity size that is roughly equivalent to atomic ion dimensions [25,26]. An interesting question for this ligand regards the feasibility of the direct insertion of the transition metal ions into the cavity. Dunbar and co-workers have observed the efficiency of formation of the $M(TBC)^+$ and $M(TBC)_2^+$ ions in radiative association experiments [25]. The observed reduction in the dimer formation efficiencies for the Co, Ni, and Cu species led to the postulate that the corresponding monomers of these metals had inserted into the cavity. The dimer formation process would then require some

Table 7
Cationic metal ligand binding energies and separations for $M(C_{12}H_6)^+$ and $M(TBC)^+$

			Binding energy (kcal/mol)[a]		R_{MX} (Å)[b]		Eff.[c]
Metal	State	Sym.	$C_{12}H_6$	TBC	$C_{12}H_6$	TBC	TBC
Ti	$^4A_1$	C_{3v}	71.0	87.0	1.108,1.347	1.084,1.293	0.23
V	$^5A''$	C_s	67.0	82.1	1.325,1.380	0.973,1.131	0.17
Cr	$^6A_1$	C_{3v}	56.8	70.5	1.018,1.190	0.868,1.016	0.23
Mn	$^7A_1$	C_{3v}	43.6	57.4	1.957,2.011	1.862,1.895	
	$^7A_2$	C_{3v}	62.4	54.1	0.998,1.104	0.953,1.043	
	$^5A'$	C_s	47.3	63.4	0.579,0.812	0.500,0.730	0.11
Fe	$^4A_1$	C_{3v}	92.2	102.4	0.617,0.822	0.575,0.763	0.09
	$^6A_1$	C_s	47.1	61.8	1.900,1.955	1.806,1.836	
Co	$^3A_1$	C_{3v}	95.2	111.9	0.501,0.664	0.432,0.572	0.027
Ni	$^2A'_1$	D_{3h}	94.3	110.8	0.0,0.0	0.0,0.0	0.011
Cu	$^1A_1$	D_{3h}	92.4	107.5	0.0,0.0	0.0,0.0	<0.02

[a] B3LYP//B3′//B3LYP/B1 zero-point corrected metal ligand binding energies. The zero-point corrections are evaluated with the B1 basis set.

[b] Equilibrium distance from the metal to the plane containing the acetylenic and ethylenic (or benzylic) C's, respectively. For C_s symmetry, there are actually three such metal–ligand plane distances for the acetylenic carbons and three for the ethylenic carbons. In those cases, only the smallest of these distances are reported.

[c] $M(TBC)_2^+$ dimer formation efficiencies in radiative association from [25].

energy to extract the ion from the ligand cavity and thus one might expect a lower formation rate. This postulate seems reasonable given the decrease in the atomic ion radius to the right of the first transition series.

The present B3LYP results for the $M(C_{12}H_6)^+$ and $M(TBC)^+$ species, provided in Table 7, agree with this postulate and other experimental observations. In particular, the Ni and Cu TBC cationic complexes are found, as postulated, to be planar species. Further, the Co cation sits only 0.4 Å above the closest plane of C atoms in the $Co(TBC)^+$ species. Thus, a second TBC ligand would have to push the first TBC ligand away from the metal in order to form the $Co(TBC)_2^+$ complex. Therefore, it seems reasonable to associate some promotion energy and correspondingly reduced efficiency for the formation of the dimer from $Co(TBC)^+$. The metal–ligand separations for the ground states of Fe and Mn are the next smallest, being on the order of 0.6 Å, and also correlate with the next lowest dimer formation efficiencies.

The most remarkable aspect of Table 7 is the overall strength of the binding for these complexes. For the $M(TBC)^+$ complexes, the binding energy is as much as 2.1 times that in the $M(C_6H_6)^+$ complexes. For ease of comparison, the B3LYP calculated binding energies are plotted in Fig. 3 for all of the species considered here.

There is also a remarkably consistent difference of

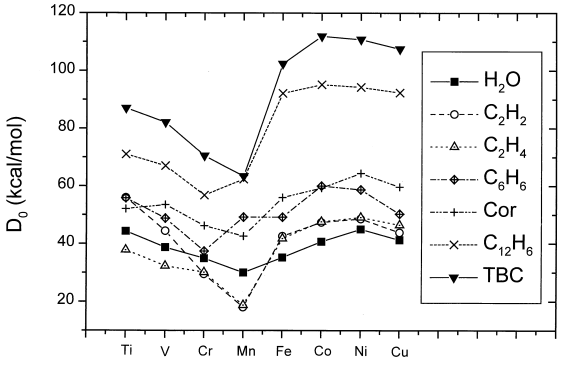

Fig. 3. Present B3LYP predictions for the metal–ligand binding energies.

about 15 kcal/mol between the $M(TBC)^+$ and $M(C_{12}H_6)^+$ binding energies. This difference is likely due to the factor of two difference in the polarizabilities of the TBC and $C_{12}H_6$ ligands. Alternatively, the differences may arise from differences in the two ligands such as the presence of ethylenic CC bonds in the $C_{12}H_6$ ligand (with a bond length of 1.36 Å) in place of the benzylic CC bonds in the TBC ligand (with a bond length of 1.43 Å).

Differences in the cavity size are quite minimal and are unlikely to contribute much to the differences in bonding energies. For example, for the $M(TBC)^+$ complexes, the side-to-side distance in the ligand is 4.760, 4.771, 4.763, and 4.726 Å for the free ligand, and the Cu, Ni, and Co, complexes, respectively. The corresponding side-to-side distances in the same $M(C_{12}H_6)^+$ complexes are 4.752, 4.750, 4.742, and 4.702 Å. The changes in other cavity bond lengths with the addition of the metal are similarly modest.

There are, however, significant out-of-plane displacements of the ligand atoms [35]. In particular, bowl shaped distortions of the TBC ligand generally occur, with the metal on the convex side of the bowl, closest to the acetylenic C atoms. The various planes of the symmetry related atoms in the TBC ligand are typically displaced from this closest plane of atoms by a few tenths of an angstrom.

Harmonic vibrational analyses have again been performed for each of the ground state complexes [35]. In this case, only the $Cr(C_{12}H_6)^+$ complex has an imaginary frequency, and we suspect that once again this is simply an indication of limitations in the B1 basis set.

In generating the results for Table 7, we have generally assumed that the orbital ordering is identical to that for the metal benzenes. That is, taking the metal–ligand axis as the z axis, the degenerate (in C_{3v} symmetry) d_{x2-y2} and d_{xy} orbitals are the lowest energy, followed by the d_{z2} orbital, and then the degenerate d_{xz} and d_{yz} orbitals. However, for the Fe $^6A_1$ states, we have doubly occupied the d_{z2} orbital, since this allows for an optimization within C_{3v} symmetry with no Jahn-Teller distortion. Attempts at doubly occupying the d_{x2-y2} or d_{xy} orbitals tended to converge to charge-transfer states which were actually lower in energy than the d^6s configuration states. The latter charge transfer states were still higher than the quartet states and so a description of their energetics is not provided here.

The relatively small binding energy for the $^7A_1$ d^5s Mn states [compared to the other $M(TBC)^+$ and $M(TC)^+$ species] is simply due to the large s orbital resulting in a large metal–ligand separation. The $^7A_2$ state corresponds to a charge transfer state where the Mn s orbital population is much lower. As a result, the metal approaches the ligand more closely and the increased metal–ligand interactions are able to overcome the charge transfer promotion energy, yielding a ground $^7A_2$ state for $Mn(TC)^+$. For $Mn(TBC)^+$ the ground state is a $^5A'$ state, with a d^6 configuration. This state has a free metal ion promotion energy of 42 kcal/mol, which roughly correlates with the difference in the binding energy of the ^{3}Co state and the ^{5}Mn state. Similarly, the promotion energy of 5 kcal/mol for the ^{4}Fe d^7 configuration roughly correlates with the difference between the ^{4}Fe and ^{3}Co binding energies.

For the Ni states we have left the d_{z2} orbital singly occupied, since this again yields a state without any Jahn-Teller distortions. Attempts to consider other Jahn-Teller distorted configurations were plagued with convergence problems. Furthermore, given the planar nature of the complex, it may be that this is actually the preferred orbital occupation. In any case, it is unlikely that leaving a different orbital unoccupied would yield a significantly lower binding energy, or a qualitatively different structure.

4. Summary

The present B3LYP predictions for the cationic transition metal–ligand binding energies for water, acetylene, ethylene, and benzene are found to generally be in reasonable agreement with CCSD(T) theoretical results and/or experimental results. Examination of the results suggests that the B3LYP results are generally accurate to within about 5 kcal/mol. It appears that larger discrepancies are generally an indication of some other failure, such as the variation

from the SCF geometries in the MCPF calculations for the metal–acetylenes [14] and metal–ethylenes [15]. The B3LYP predicted metal–acetylene and metal–ethylene binding energies are remarkably similar for all but Ti and V, where the acetylenic binding energies are 10–20 kcal/mol greater.

The present B3LYP calculations suggest that the cationic binding in the metal–coronenes is very similar to that in the metal–benzenes. The increased polarizability of coronene does, however, lead to an increase in the binding energy by 5 kcal/mol on average. In contrast, the metal–tribenzocyclyne binding energies are about a factor of 2 greater than the metal–benzene binding energies, with the Co, Ni, and Cu, metal–tribenzocyclyne binding energies as large as 110 kcal/mol. Furthermore, the B3LYP calculations suggest that both $Ni(TBC)^+$ and $Cu(TBC)^+$ are planar species with the metal inserting directly into the ligand cavity, as first postulated by Dunbar and co-workers [25,26].

Acknowledgements

The support of this research by the donors of the Petroleum Research Fund, administered by the American Chemical Society, is gratefully acknowledged, as are valuable discussions with Professor R. C. Dunbar.

References

[1] A.D. Becke, J. Chem. Phys. 98 (1993) 5648.
[2] A. Ricca, C.W. Bauschlicher Jr., Theor. Chim. Acta 92 (1995) 123.
[3] M. Sodupe, V. Branchadell, M. Rosi, C.W. Bauschlicher Jr., J. Phys. Chem. A 101 (1997) 7854.
[4] C.W. Bauschlicher Jr., P. Maitre, J. Phys. Chem. 99 (1995) 3444; 99 (1995) 6836.
[5] J.E. Bushnell, P. Maitre, P.R. Kemper, M.T. Bowers, J. Chem. Phys. 106 (1997) 10153.
[6] C.-N. Yang, S.J. Klippenstein, J. Phys. Chem. A 103 (1999) 1094.
[7] V. Ryzhov, C.-N. Yang, S.J. Klippenstein, R.C. Dunbar, Int. J. Mass Spectrom. Ion Processes 185/186/187 (1999) 913.
[8] A. Gapeev, C.-N. Yang, S.J. Klippenstein, R.C. Dunbar, J. Phys. Chem., 104(2000) 3246.
[9] F. Meyer, F.A. Khan, P.B. Armentrout, J. Am. Chem. Soc. 117 (1995) 9740.
[10] C.W. Bauschlicher Jr., H. Partridge, S.R. Langhoff, J. Phys. Chem. 96 (1992) 3273.
[11] D. Stockigt, J. Schwarz, H. Schwarz, J. Phys. Chem. 100 (1996) 8786.
[12] M. Rosi, C.W. Bauschlicher Jr., J. Chem. Phys. 90 (1989) 7264.
[13] M. Rosi, C.W. Bauschlicher Jr., J. Chem. Phys. 92 (1990) 1876.
[14] M. Sodupe, C.W. Bauschlicher Jr., J. Phys. Chem. 95 (1991) 8640.
[15] M. Sodupe, C.W. Bauschlicher, S.R. Langhoff, H. Partridge, J. Phys. Chem. 96 (1992) 2118.
[16] C.W. Bauschlicher Jr., S.R. Langhoff, H. Partridge, in B.S. Freiser (Ed.), Organometallic Ion Chemistry, Kluwer, Dordrecht, 1996, pp. 47–87.
[17] E. Magnusson, N.W. Moriarty, J. Comp. Chem. 14 (1993) 961.
[18] M. Trachtman, G.D. Markham, J.P. Glusker, P. George, C.W. Bock, Inorg. Chem. 37 (1998) 4421.
[19] N.F. Dalleska, K. Honma, L.S. Sunderlin, P.B. Armentrout, J. Am. Chem. Soc. 116 (1994) 3519.
[20] B.L. Kickel, P.B. Armentrout, in B.S. Freiser (Ed.), Organometallic Ion Chemistry, Kluwer, Dordrecht, 1996, pp. 1–45.
[21] M.R. Sievers, L.M. Jarvis, P.B. Armentrout, J. Am. Chem. Soc. 120 (1998) 1891.
[22] T.F. Magnera, D.E. David, J. Michl, J. Am. Chem. Soc. 111 (1989) 4100; T.F. Magnera, D.E. David, D. Stulik, R.G. Orth, H.T. Jonkman, J. Michl, J. Am. Chem. Soc. 111 (1989) 5036.
[23] P.J. Marinelli, R.R. Squires, J. Am. Chem. Soc. 111 (1989) 4101.
[24] P.B. Pozniak, R.C. Dunbar, J. Am. Chem. Soc. 119 (1997) 10439.
[25] R.C. Dunbar, G.T. Uechi, D. Solooki, C.A. Tessier, W. Youngs, B. Asamoto, J. Am. Chem. Soc. 115 (1993) 12477.
[26] R.C. Dunbar, D. Solooki, C.A. Tessier, W.J. Youngs, B. Asamoto, Organometallics 10 (1991) 52.
[27] GAUSSIAN 98, revision A.6, M.J. Frisch, G.W. Trucks, H.B. Schlegel, G.E. Scuseria, M.A. Robb, J.R. Cheeseman, V.G. Zakrzewski, J.A. Montgomery Jr., R.E. Stratmann, J.C. Burant, S. Dapprich, J.M. Millam, A.D. Daniels, K.N. Kudin, M.C. Strain, O. Farkas, J. Tomasi, V. Barone, M. Cossi, R. Cammi, B. Mennucci, C. Pomelli, C. Adamo, S. Clifford, J. Ochterski, G.A. Petersson, P.Y. Ayala, Q. Cui, K. Morokuma, D.K. Malick, A.D. Rabuck, K. Raghavachari, J.B. Foresman, J. Cioslowski, J.V. Ortiz, B.B. Stefanov, G. Liu, A. Liashenko, P. Piskorz, I. Komaromi, R. Gomperts, R.L. Martin, D.J. Fox, T. Keith, M.A. Al-Laham, C.Y. Peng, A. Nanayakkara, C. Gonzalez, M. Challacombe, P.M.W. Gill, B. Johnson, W. Chen, M.W. Wong, J.L. Andres, C. Gonzalez, M. Head-Gordon, E.S. Replogle, J.A. Pople, Gaussian, Inc., Pittsburgh, PA, 1998.
[28] C.E. Moore, Atomic Energy Levels, U.S. National Bureau of Standards Circular 467, NBS, Washington, DC, Vol. I, 1949; Vol. II, 1952.
[29] C.W. Bauschlicher Jr., S.R. Langhoff, Int. Rev. Phys. Chem. 9 (1990) 149.
[30] K. Raghavachari, G.W. Trucks, J. Chem. Phys. 91 (1989) 2457.
[31] T. Ziegler, J. Li, Can. J. Chem. 72 (1994) 783.

[32] T.V. Russo, R.L. Martin, P.J. Hay, J. Chem. Phys. 101 (1994) 7729.
[33] M.C. Holthausen, C. Heinemann, H.H. Cornehl, W. Koch, H. Schwarz, J. Chem. Phys. 102 (1995) 4931.
[34] C.W. Bauschlicher Jr., A. Ricca, H. Partridge, S.R. Langhoff, in D.P. Chong (Ed.), Recent Advances in Density Functional Methods, Part II, World Scientific, Singapore, 1995, p. 165.
[35] EXCEL tables containing these frequencies are available from S.J.K. via e-mail to *sjk5@po.cwru.edu*, as are text files containing the optimized geometries in Cartesian coordinates.